Effective-mass approximation for shallow donors in uniaxial indirect band-gap crystals and application to 4*H*-SiC

I. G. Ivanov
Department of Physics and Measurement Technology, Linköping University, S-58183 Linköping, Sweden

A. Stelmach
Ericsson Technology Licensing AB, Nya Vattentornet, S-22188 Lund, Sweden

M. Kleverman
Sony Ericsson Mobile Communication AB, Nya Vattentornet, S-22188 Lund, Sweden

E. Janzén
Department of Physics and Measurement Technology, Linköping University, S-58183 Linköping, Sweden
(Received 21 December 2004; revised manuscript received 28 November 2005; published 18 January 2006)

The effective-mass theory is applied for description of the electronic states of shallow donors in indirect band-gap uniaxial crystals, which have three different components of the electron effective-mass tensor, and two different components of the tensor of the dielectric constant. The Hamiltonian in the resulting Schrödinger equation for the envelope function has D_{2h} symmetry and, after proper parametrization, a nonvariational numerical method is used for its solution. Two particular cases of $D_{\infty h}$ symmetry are identified and discussed separately. The comparison between theory and experiment for the 4*H* polytype of silicon carbide is revised using the least-squares method to determine the binding energies of the ground state of the most shallow nitrogen donor in this material, its valley-orbit split-off counterpart, and the mean value of the dielectric constant, and completed with calculation of the theoretical transition probabilities. In addition, the lowest-lying binding energies of the states, between which optical transitions are allowed, are calculated on a grid of values of the two parameters describing the anisotropy and the tabulated values can be used for interpolation to describe other materials.

DOI: 10.1103/PhysRevB.73.045205 PACS number(s): 71.55.−i, 78.55.Hx

I. INTRODUCTION

It is well known that the effective-mass theory (EMT) is an indispensable tool in understanding the electronic structure of shallow donors and acceptors in semiconductors. The EMT developed originally by Kohn and Luttinger[1] has been subsequently employed in accurate numerical calculations performed by Faulkner[2] for cubic semiconductors with indirect band gap and prolate-spheroid conduction bands, such as silicon and germanium. The Hamiltonian in the resulting Schrödinger equation for the envelope function has cylindrical symmetry, $D_{\infty h}$ in this case. Approximate formulas for the binding energies of excitons in uniaxial crystals have been worked out by Gerlach and Pollmann.[3] However, in their work they implicitly assume direct band-gap semiconductor, and the resulting Hamiltonian also has cylindrical symmetry. Hence, Faulkner's theory is directly applicable, provided a suitable parametrization of the Schrödinger equation is made.

The most general case—that of uniaxial semiconductor with indirect band gap—has not been considered in detail so far and will be worked out in this paper. We shall assume that the lowest conduction band is nondegenerate and separated enough in energy from the next-lowest conduction band, so that the motion of the donor electron can be described using the effective-mass tensor only for the lowest conduction band. An important example of such a crystal is the 4*H* polytype of silicon carbide (4*H*-SiC), which has drawn a lot of attention during the past decade due to its potential for high-power and high-temperature applications. The optical selection rules for this polytype were recently discussed.[4] A preliminary account on the application of the current theory to explain the observed donor excited states was also published[5] but only a few states were computed at that time. Another assumption, which is implicitly built in our theory, is the validity of the one-valley approximation. This leads to neglecting the valley-orbit interaction, similar to the theory used by Faulkner.[2] However, it is well known that the valley-orbit interaction is strongly pronounced mainly for the ground state of the donor, hence, the theory is expected to provide an accurate description of the excited states. The energies of the ground state and its valley-orbit split counterpart are evaluated by comparison of the theory with the experiment.

Before proceeding with the main scope, the following two remarks are appropriate. First, the theory cannot be applied without modifications if the lowest conduction band, being single, is nonparabolic. An example is another common polytype of SiC, namely, 6*H*-SiC, which has the so-called "camel-back" structure near the conduction band minimum.[6] The second remark concerns the application of the theory to shallow acceptors. The topmost valence band is usually nondegenerate, because the crystal field and the spin-orbit interaction remove any degeneracy in uniaxial crystals. However,

the energy distance between the topmost valence bands is usually much smaller than the acceptor binding energy (at least, this is the case in 4*H*-SiC), hence the theory cannot be applied using only the effective-mass tensor for the holes from the topmost valence band.

Thus, we develop the effective-mass theory for donor excited states in uniaxial semiconductors with simple parabolic, but anisotropic conduction band. The theory is described in Sec. II. All quantitative results are obtained using numerical calculations, however, special concern is given to group-theoretical consideration, which allows classification of the donor wave functions by symmetry and greatly reduces the efforts in the numerical calculation. Since the case of cylindrical symmetry considered by Faulkner[2] is just a particular case in our calculation, we investigate also the accuracy of his tables and show that some of his results need reevaluation. We tabulate also another cylindrically symmetric case, which has been treated only approximately so far.[3] In Sec. III, our theoretical approach is compared to other work, and the theory is used to fit the experimental data available for 4*H*-SiC and compute the observed transition probabilities. Finally, Sec. IV summarizes the conclusions.

II. EFFECTIVE-MASS THEORY IN UNIAXIAL INDIRECT BAND-GAP CRYSTALS

The one-valley effective-mass approximation will be built for the general case of three different components of the electron effective-mass tensor and two different components of the tensor of the dielectric constant.

A. Parametrization of the Schrödinger equation

The Schrödinger equation for the envelope function in the one-valley approximation is usually written in a coordinate system with the *OZ* axis oriented along the crystal **c** axis (cf. Refs. 3 and 4),

$$H_1\phi_1 = -\frac{\hbar^2}{2}\left(\frac{1}{m_X}\frac{\partial^2}{\partial X^2} + \frac{1}{m_Y}\frac{\partial^2}{\partial Y^2} + \frac{1}{m_Z}\frac{\partial^2}{\partial Z^2} + \frac{e^2}{\sqrt{\varepsilon_\parallel \varepsilon_\perp}\sqrt{X^2 + Y^2 + \frac{\varepsilon_\perp}{\varepsilon_\parallel}Z^2}}\right)\phi_1 = E\phi_1. \quad (1)$$

Here H_1 denotes the effective-mass one-valley Hamiltonian, e is the electron charge, m_X, m_Y, and m_Z are the electron effective masses along the *OX*, *OY*, and *OZ* coordinate axes, $\varepsilon_\parallel$ and $\varepsilon_\perp$ are the dielectric constants along and perpendicular to the crystal axis (**c** axis), and ϕ_1 is the envelope function.

For the sake of the following computation it is essential to reorient the coordinate axis so that in the new coordinate system *Oxyz* the *Oz* axis is along the direction corresponding to the largest anisotropy. More strictly, the following quantities of dimension of mass (called for convenience generalized masses) are compared:

$$m_1 = m_X, \quad m_2 = m_Y, \quad m_3 = \frac{\varepsilon_\parallel}{\varepsilon_\perp}m_Z. \quad (2)$$

Our convention is that the largest generalized mass determines the direction of the *Oz* axis, and the smallest one, that of the *Oy* axis. For convenience, these two generalized masses can be relabelled as m_z and m_y, respectively, and the remaining one as m_x. Thus, $m_y < m_x < m_z$. The following coordinate transformation can be used then to bring the kinetic energy term in Eq. (1) to a spherically symmetric term:

$$\xi = \sqrt{\frac{m_x}{m_y}}x, \quad \eta = y, \quad \zeta = \sqrt{\frac{m_z}{m_y}}z. \quad (3)$$

Using spherical coordinates, $\xi = r\cos\varphi\sin\theta$, $\eta = r\sin\varphi\sin\theta$, and $\zeta = r\cos\theta$, and introducing as defined below the units for length and energy a and R_{eff}, respectively, Eq. (1) can be transformed to dimensionless form:

$$\left(-\triangle_\rho - \frac{2}{\rho\sqrt{1-\alpha\cos^2\theta - \beta\sin^2\theta\cos^2\varphi}}\right)\phi = \epsilon\phi. \quad (4)$$

Here $\rho = r/a$ and $\epsilon = E/R_{\text{eff}}$ are the dimensionless measures for length and energy, respectively, $\triangle_\rho$ is the Laplacian operator in spherical coordinates with respect to the variables ρ, θ (the polar angle) and φ (the azimuthal angle), and

$$\alpha = 1 - m_y/m_z \leqslant 1, \quad \beta = 1 - m_y/m_x \leqslant \alpha \quad (5)$$

are the two parameters describing the anisotropy. Note that $\alpha = 0$ describes the spherically symmetric case.

The units for length and energy, called usually effective Bohr radius and effective Rydberg, respectively, are defined as follows:

$$a = \frac{\varepsilon\hbar^2}{m_y e^2}, \quad (6)$$

$$R_{\text{eff}} = \frac{m_y}{\varepsilon^2}\frac{e^4}{2\hbar^2}, \quad (7)$$

where $\varepsilon \equiv \sqrt{\varepsilon_\perp \varepsilon_\parallel}$. These are the two quantities containing the material parameters ε and m_y.

It is easily verified that in the general case the symmetry group of the effective-mass Hamiltonian is D_{2h}. However, for $\beta = 0$ (i.e., $m_y = m_x < m_z$) and for $\beta = \alpha$ ($m_x = m_z > m_y$), the symmetry of the Hamiltonian elevates to $D_{\infty h}$. These cases will be referred to further as cylindrically symmetric cases.

B. Symmetry consideration and numerical implementation

The numerical method used to solve Eq. (4) has been used previously for calculating acceptor states[7,8] and is described in detail in Ref. 9. For the sake of clarity, a brief account on the main steps will be given when necessary. This method has the obvious advantage that no trial function needs to be constructed *a priori*.

The anisotropy of the Hamiltonian in Eqs. (1) and (4) is characterized by the function

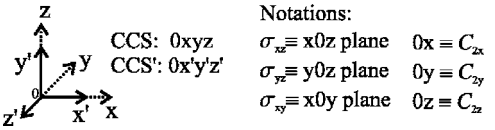

FIG. 1. The mutual orientation of the two coordinate systems CCS and CCS′ and some notations used in the theory.

$$f(\theta,\varphi)=\frac{1}{\sqrt{1-\alpha\cos^2\theta-\beta\sin^2\theta\cos^2\varphi}}, \tag{8a}$$

$$f(\theta',\varphi')=\frac{1}{\sqrt{1-\beta\sin^2\theta'-(\alpha-\beta)\sin^2\theta'\sin^2\varphi'}}. \tag{8b}$$

Here f is expressed as a function of the polar and the azimuthal angles in the original coordinate system (θ,φ) and in the "primed" coordinate system (the corresponding angles are denoted θ',φ'), which is defined in Fig. 1, hence the two alternative expressions (8a) and (8b). The rest of the Hamiltonian is invariant in the two coordinate systems. The need for using two coordinate systems will be clarified below.

Let us consider the two cylindrically symmetric cases. When $\beta=0$ (Faulkner's case) we use the spherical harmonics related to CCS (see the notation definitions in Fig. 1) in the expansion of the wave function. According to Eq. (8a), the function f does not depend on φ in this case, therefore different values of the projection of the orbital momentum m do not mix (m is a good quantum number). However, if $\beta=\alpha$, f is independent of φ', not of φ, according to Eqs. (8), and we must use the spherical harmonics as defined in the primed coordinate system. Obviously, in this case the Oz' axis is oriented along the symmetry axes of the system, so that the projection of the orbital momentum with respect to this axis is again a good quantum number. Note that the extreme limit of the first case ($m_x=m_y<m_z$), that is, when $m_z\to\infty$ is the two-dimensional case (often called two-dimensional H atom, or adiabatic case).[1] On the other hand, for the second cylindrically symmetric case($m_x=m_z>m_y$), the extreme limit $m_x=m_z\to\infty$ is the one-dimensional case (called also one-dimensional H atom).[10] The question which of the two coordinate systems should be used for intermediate values of β will be postponed until Sec. II D.

Each wave function ϕ, solution of Eqs. (1) and (4), is expanded in series in the normalized spherical harmonics $Y_l^m(\theta,\varphi)$. The coefficients in this expansion (functions of ρ) are denoted by $U_l^m(\rho)/\rho$ as in Ref. 9. In the general case only the parity remains a good quantum number.[2,9]

Using the well-known projector-operators technique[11] and the symmetry properties of the spherical harmonics, it is quite straightforward to find the explicit form of the wave function for each irreducible representation. Its expansion involves linear combinations of spherical harmonics, denoted here as $\Upsilon_l^{m\,\Gamma_i}(\theta,\varphi)$ and determined by the irreducible representation Γ_i of the symmetry group of the Hamiltonian (D_{2h}) according to which the wave function transforms. The irreducible representations Γ_i of the group D_{2h} together with the corresponding sets of functions $\Upsilon_l^{m\,\Gamma_i}(\theta,\varphi)$ are listed in Table I. For example, according to the table the series expansion of the functions transforming as the fully symmetric Γ_1^+ has the form

$$\begin{aligned}\phi_n^{\Gamma_1^+}(\rho,\theta,\varphi)&=\sum_{l,m}\frac{U_{l,n}^m(\rho)}{\rho}\Upsilon_l^{m\,\Gamma_1^+}(\theta,\varphi)\\&=\sum_{l=0(2)}^{\infty}\frac{U_{l,n}^0(\rho)}{\rho}Y_l^0(\theta,\varphi)\\&\quad+\sum_{l=2(2)}^{\infty}\sum_{m=0(2)}^{l}\frac{U_{l,n}^m(\rho)}{\rho}\frac{Y_l^m(\theta,\varphi)+Y_l^{-m}(\theta,\varphi)}{\sqrt{2}},\end{aligned} \tag{9}$$

where the integer index n enumerates the states. Since l and $m\leqslant l$ must both be even, hence the notation "(2)" in the lower index of the sums. For simplicity we will often omit the indices denoting the representation and the state number.

The irreducible representations in Table I are labelled using the notations of Ref. 12 (for convenience another common set of notations is shown in parentheses). All representations of D_{2h} are one dimensional, thus no symmetry-imposed energy degeneracies are expected (apart from accidental degeneracies).

For any representation the norm of the wave function is given by

TABLE I. Irreducible representations of D_{2h} and the normalized linear combinations of spherical harmonics involved in the expansion of the wave function for each specific representation. E and I denote the identity and the inversion operator, respectively, the other notations of the symmetry elements are clarified in Fig. 1.

D_{2h}	E	C_{2x}	C_{2z}	C_{2y}	I	σ_{xz}	σ_{yz}	σ_{xy}	$\Upsilon_l^{m\,\Gamma_i}(\theta,\varphi)$
$\Gamma_1^+(A_{1g})$	1	1	1	1	1	1	1	1	$Y_l^0,(Y_l^m+Y_l^{-m})/\sqrt{2}$, l-even, m-even
$\Gamma_2^+(B_{2g})$	1	−1	−1	1	1	1	−1	−1	$(Y_l^m-Y_l^{-m})/\sqrt{2}$, l-even, m-odd
$\Gamma_3^+(B_{1g})$	1	−1	1	−1	1	−1	−1	1	$(Y_l^m-Y_l^{-m})/\sqrt{2}$, l-even, m-even
$\Gamma_4^+(B_{3g})$	1	1	−1	−1	1	−1	1	−1	$(Y_l^m+Y_l^{-m})/\sqrt{2}$, l-even, m-odd
$\Gamma_1^-(A_{1u})$	1	1	1	1	−1	−1	−1	−1	$(Y_l^m-Y_l^{-m})/\sqrt{2}$, l-odd, m-even
$\Gamma_2^-(B_{2u})$	1	−1	−1	1	−1	−1	1	1	$(Y_l^m+Y_l^{-m})/\sqrt{2}$, l-odd, m odd
$\Gamma_3^-(B_{1u})$	1	−1	1	−1	−1	1	1	−1	$Y_l^0,(Y_l^m+Y_l^{-m})/\sqrt{2}$, l-odd, m-even
$\Gamma_4^-(B_{3u})$	1	1	−1	−1	−1	1	−1	1	$(Y_l^m-Y_l^{-m})/\sqrt{2}$, l-odd, m odd

$$\|\phi_n\|^2 = \sum_{l,m} \int_0^\infty [U_{l,n}^m(\rho)]^2 d\rho, \tag{10}$$

where the summation extends over all allowed values of l and m for that representation.

Feeding back the expansion of the wave function in Eq. (4) and using the fact that the spherical harmonics are eigenfuctions of the angular part of the Laplacian operator with eigenvalues $l(l+1)$, the following system of coupled differential equations for the functions $U_l^m(\rho)$ is easily obtained:

$$-\frac{d^2U_l^m}{d\rho^2} + \frac{l(l+1)}{\rho^2}U_l^m - \frac{2}{\rho}\sum_{l',m'\neq l,m} U_{l'}^{m'} Z_{l,l'}^{m,m'} = \epsilon U_l^m. \tag{11}$$

The matrix elements $Z_{l,l'}^{m,m'}$ are defined as follows:

$$Z_{l,l'}^{m,m'} = \int_0^\pi d\theta \int_0^{2\pi} d\varphi \Upsilon_l^m(\theta,\varphi)\Upsilon_{l'}^{m'}(\theta,\varphi) f(\theta,\varphi). \tag{12}$$

Obviously, there is one such system of differential equations for each representation. The calculation of the matrix elements is explained in more detail in the Appendix.

The problem of solving the infinite system of differential equations (11) is reduced to a problem of finding the eigenvalues and the eigenvectors of a Hermitian (in our case even symmetric) matrix, as described in Ref. 9. The functions $U_l^m(\rho)$ are evaluated on a radial mesh in the interval $0<\rho<\rho_{\max}=N_r h$, the boundary conditions $U_l^m(0)=U_l^m[(N_r+1)h]=0$ are imposed, and the derivatives are represented by finite elements. Here N_r denotes the number of points on the mesh, and $h=\rho_{\max}/N_r$ is the step. In order to make the resulting algebraic system of equations finite, the expansion of the wave functions is restricted to some maximum value of l, $L_{\max}$. The total number of functions involved in the expansion is $N_f=1/2([L_{\max}]/2)[([L_{\max}]/2)+1]$, where $[L_{\max}]$ denotes the largest even number not exceeding $L_{\max}$. The resulting large eigenvalue problem (of dimension $N=N_rN_f$) is solved using a variation of Lánczos procedures with reorthogonalization.[13]

Among the eight sets of states corresponding to the eight irreducible representations, four are of greater importance, because optical transitions between them are allowed (for the selection rules, see Ref. 4). These are the fully symmetric S-like states transforming as Γ_1^+, and the P-like states, transforming as Γ_3^-, Γ_2^-, and Γ_4^-, and called here P_0-like, P_--like, and P_+-like states, respectively. The notations P_0, P_y, and P_z were used previously,[4] but in view of the necessity for a different choice of the coordinate system it is not convenient to bind the notations with the coordinate axis.

C. Results of the calculation and discussion

It is convenient to consider the two cases of cylindrical symmetry ($\beta=0$ and $\beta=\alpha$) separately from the general case $0<\beta<\alpha$, because the Hamiltonian in the former two cases has higher symmetry, $D_{\infty h}$, and the calculation can be performed with enhanced accuracy. In all cases the number of points used on the radial mesh is $N_r=2048$, however, values of $L_{\max}$ up to 28 (29) were used in the cylindrically symmetric cases for even (odd) states, whereas in the general case $L_{\max}=12(13)$ were used.

1. Cylindrically symmetric cases

Within our model both cylindrically symmetric cases are described using a single parameter $0\leqslant\alpha=1-m/M<1$, defined via the ratio of the smaller mass m to the larger mass M. The only difference between the two cases is in the anisotropy function [cf. Eqs. (8)]

$$f(\theta) = (1-\alpha\cos^2\theta)^{-\frac{1}{2}}, \quad \beta=0, \tag{13a}$$

$$f(\theta') = (1-\alpha\sin^2\theta')^{-\frac{1}{2}}, \quad \beta=\alpha. \tag{13b}$$

The case $\beta=0$ differs from the case $\beta=\alpha$ also in that the two equal masses are the smallest in the first case and the largest in the second one. The extreme cases ($\alpha=1$) resulting in a two- or one-dimensional hydrogen atom, have been studied elsewhere and will be disregarded here.[1,10,14]

Table II presents the results from the calculation for the nine lowest-lying S-like, P_0-like, and $P_\pm$-like states, using the same values of $\gamma=(1-\alpha)$ as in Ref. 2. The notations in the middle column represent the well-known states of the spherically symmetric case ($\gamma=1$, or $\alpha=0$) and are given as limits to the corresponding states. The left part of the table lists the binding energies of the states for $\beta=0$ (Faulkner's case), which can be compared directly to the tables from Ref. 2. The right part of the table represents the case $\beta=\alpha$. This case has been treated using approximate formulas in Ref. 3 but not tabulated accurately before. To avoid confusion, we note that our definition of α is equivalent to the definitions in Refs. 2 and 3 for $\beta=0$, but differs from the definition of Ref. 3 for $\beta=\alpha$ (Faulkner does not consider this case). If their parameter is denoted as $\alpha'=1-M/m$ (cf. Ref. 3), then for $\beta=\alpha$ the relation to our α is $\alpha'=-\alpha/(1-\alpha)$, $-\infty<\alpha'<0$.

We notice that our (absolute) values for $\beta=0$ are systematically higher than those in Ref. 2, i.e., our binding energies are lower. The disagreement increases towards smaller values of $\gamma^{1/3}$, and also for a fixed value of γ with increasing the number of the excited state. This is a consequence of the different values of $L_{\max}$ in the two calculations that are compared [$L_{\max}=4(5)$ in Ref. 2]. However, the agreement is excellent for $\gamma^{1/3}>0.6$. We found that $L_{\max}$ must be increased up to 28 (29) in order to ensure convergence to within three digits for $\gamma=0.1$, whereas for $\gamma>0.2$ $L_{\max}=14(15)$ seems to be enough. Thus, our calculation for Si ($\gamma^{1/3}\cong 0.59$) yields the same values as the published ones,[15] calculated with $L_{\max}=10(11)$. However, all values for $\gamma^{1/3}\leqslant 0.5$ are calculated with $L_{\max}=28(29)$.

The results from Table II are plotted as a graph in Figs. 2 and 3. The points in these and all subsequent graphs are connected with straight lines intentionally, in order to give a feeling for the errors committed when using linear interpolation between them. The significantly steeper increase in the binding energies on the left-hand side of the figures, if compared to those from Ref. 2 is obvious. Another difference concerns the ordering of the excited states. Here we have adopted a notation, which classifies the state according to the

TABLE II. Binding energies (in units of R_{eff}) of the lowest S-like ($l=0$, $m=0$), P_0-like ($l=1$, $m=0$), and $P_{\pm}$-like states ($l=1$, $m=\pm 1$) for the two cases of cylindrical symmetry, $\beta=0$ and $\beta=\alpha$. The left-hand part of the table ($\beta=0$) contains the improved values of the binding energies presented in Ref. 2, and the limiting case as $\gamma\rightarrow 0$ is the two-dimensional case. On the right-hand side of the table ($\beta=\alpha$) are the binding energies for the case with two equal masses, which are larger than the third one. The limit as $\gamma\rightarrow 0$ is the one-dimensional case. Both cases have the same limit at $\gamma=1$, the spherically symmetric case, the states of which are displayed in the middle column. The energies of these states are trivial, thus only their labels are given. When two labels are listed, the one to the left relates to the case $\beta=0$, and the one to the right to the case $\beta=\alpha$.

$\beta=0$ $\gamma^{1/3}=(1-\alpha)^{1/3}$										$\beta=\alpha$ $\gamma^{1/3}=(1-\alpha)^{1/3}$								
0.1	0.2	0.3	0.4	0.5	0.6	0.7	0.8	0.9	1.0	0.9	0.8	0.7	0.6	0.5	0.4	0.3	0.2	0.1
									S-like states									
3.23	2.71	2.321	2.011	1.760	1.553	1.379	1.233	1.108	$1S$	1.231	1.540	1.968	2.578	3.487	4.922	7.388	12.3	25.1
2.16	1.39	0.9604	0.7051	0.5436	0.4375	0.3656	0.3151	0.2782	$2S$	0.3090	0.3921	0.5131	0.6971	0.9921	1.501	2.473	4.67	11.6
1.70	0.962	0.6056	0.4143	0.3033	0.2353	0.1905	0.1577	0.1319	$3D_0,3S$	0.1392	0.1797	0.2403	0.3351	0.4926	0.7759	1.348	2.74	7.55
1.40	0.731	0.4316	0.2842	0.2202	0.1857	0.1582	0.1374	0.1223	$3S,3D_0$	0.1268	0.1451	0.1665	0.2000	0.2997	0.4849	0.8728	1.86	5.54
1.19	0.583	0.3293	0.2448	0.1901	0.1432	0.1125	0.0911	0.0750	$4D_0,4S$	0.0791	0.1034	0.1403	0.1909	0.2214	0.3353	0.6194	1.37	4.32
1.03	0.481	0.2824	0.2033	0.1396	0.1056	0.0879	0.0763	0.0683	$4S,4D_0$	0.0708	0.0808	0.0938	0.1331	0.2028	0.2578	0.4660	1.06	3.50
0.900	0.406	0.2575	0.1584	0.1175	0.0951	0.0748	0.0598	0.0486	$5D_0,5S$	0.0510	0.0673	0.0920	0.1092	0.1474	0.2467	0.3650	0.853	2.91
0.797	0.349	0.2120	0.1388	0.1034	0.0762	0.0635	0.0542	0.0465	$5G_0$	0.0466	0.0545	0.0657	0.0954	0.1303	0.1903	0.3034	0.703	2.47
0.711	0.321	0.1781	0.1252	0.0879	0.0719	0.0568	0.0484	0.0434	$5S,5D_0$	0.0449	0.0510	0.0639	0.0759	0.1121	0.1592	0.2943	0.591	2.13
									P_0-like states									
2.50	1.73	1.254	0.9390	0.7216	0.5662	0.4521	0.3664	0.3009	$2P_0$	0.2825	0.3207	0.3657	0.4190	0.4824	0.5581	0.6485	0.756	0.879
1.89	1.12	0.7231	0.4980	0.3595	0.2695	0.2083	0.1653	0.1342	$3P_0$	0.1260	0.1450	0.1697	0.2030	0.2487	0.3130	0.4050	0.540	0.731
1.53	0.823	0.4941	0.3224	0.2234	0.1622	0.1224	0.0953	0.0763	$4P_0,4F_0$	0.0732	0.0864	0.1035	0.1271	0.1615	0.2132	0.2938	0.425	0.629
1.29	0.644	0.3666	0.2300	0.1548	0.1158	0.0985	0.0843	0.0724	$4F_0,4P_0$	0.0703	0.0803	0.0928	0.1077	0.1252	0.1585	0.2280	0.349	0.551
1.11	0.524	0.2860	0.1742	0.1364	0.1094	0.0811	0.0622	0.0492	$5P_0,5F_0$	0.0473	0.0567	0.0693	0.0874	0.1141	0.1427	0.1843	0.295	0.488
0.965	0.438	0.2310	0.1624	0.1143	0.0797	0.0629	0.0535	0.0461	$5F_0,5P_0$	0.0447	0.0509	0.0588	0.0692	0.0877	0.1229	0.1645	0.255	0.436
0.851	0.374	0.1962	0.1371	0.0907	0.0746	0.0580	0.0440	0.0345	$6P_0,6F_0$	0.0332	0.0403	0.0500	0.0639	0.0800	0.0999	0.1528	0.223	0.392
0.758	0.323	0.1911	0.1122	0.0882	0.0607	0.0453	0.0382	0.0325	$6H_0$	0.0322	0.0375	0.0438	0.0519	0.0688	0.0953	0.1298	0.197	0.355
0.680	0.283	0.1616	0.1107	0.0707	0.0544	0.0437	0.0366	0.0317	$6F_0,6P_0$	0.0309	0.0350	0.0405	0.0496	0.0607	0.0823	0.1167	0.189	0.323
									$P_{\pm}$-like states									
0.428	0.407	0.3841	0.3616	0.3400	0.3195	0.3003	0.2823	0.2656	$2P_{\pm}$	0.3210	0.4215	0.5686	0.7929	1.153	1.774	2.954	5.59	13.6
0.375	0.311	0.2542	0.2107	0.1782	0.1550	0.1388	0.1272	0.1184	$3P_{\pm}$	0.1430	0.1891	0.2581	0.3665	0.5468	0.8716	1.526	3.10	8.49
0.333	0.256	0.1930	0.1501	0.1237	0.1087	0.0956	0.0833	0.0721	$4F_{\pm},4P_{\pm}$	0.0808	0.1075	0.1483	0.2135	0.3245	0.5302	0.9608	2.05	6.08
0.298	0.217	0.1549	0.1261	0.1114	0.0938	0.0805	0.0721	0.0666	$4P_{\pm},4F_{\pm}$	0.0733	0.0865	0.1027	0.1406	0.2167	0.3606	0.6702	1.49	4.67
0.268	0.188	0.1358	0.1135	0.0876	0.0718	0.0620	0.0538	0.0464	$5F_{\pm},5P_{\pm}$	0.0519	0.0695	0.0967	0.1229	0.1557	0.2628	0.4982	1.14	3.75
0.243	0.166	0.1280	0.0915	0.0726	0.0624	0.0529	0.0464	0.0426	$5P_{\pm},5F_{\pm}$	0.0469	0.0555	0.0682	0.1000	0.1484	0.2008	0.3869	0.907	3.10
0.221	0.147	0.1089	0.0814	0.0666	0.0529	0.0447	0.0383	0.0326	$6F_{\pm},6P_{\pm}$	0.0362	0.0487	0.0665	0.0811	0.1176	0.1814	0.3102	0.742	2.62
0.201	0.145	0.0952	0.0749	0.0578	0.0496	0.0423	0.0367	0.0319	$6H_{\pm}$	0.0328	0.0392	0.0507	0.0749	0.1007	0.1588	0.2549	0.620	2.25
0.185	0.132	0.0936	0.0654	0.0542	0.0439	0.0375	0.0324	0.0295	$6P_{\pm},6F_{\pm}$	0.0322	0.0375	0.0475	0.0588	0.0922	0.1290	0.2254	0.528	1.95

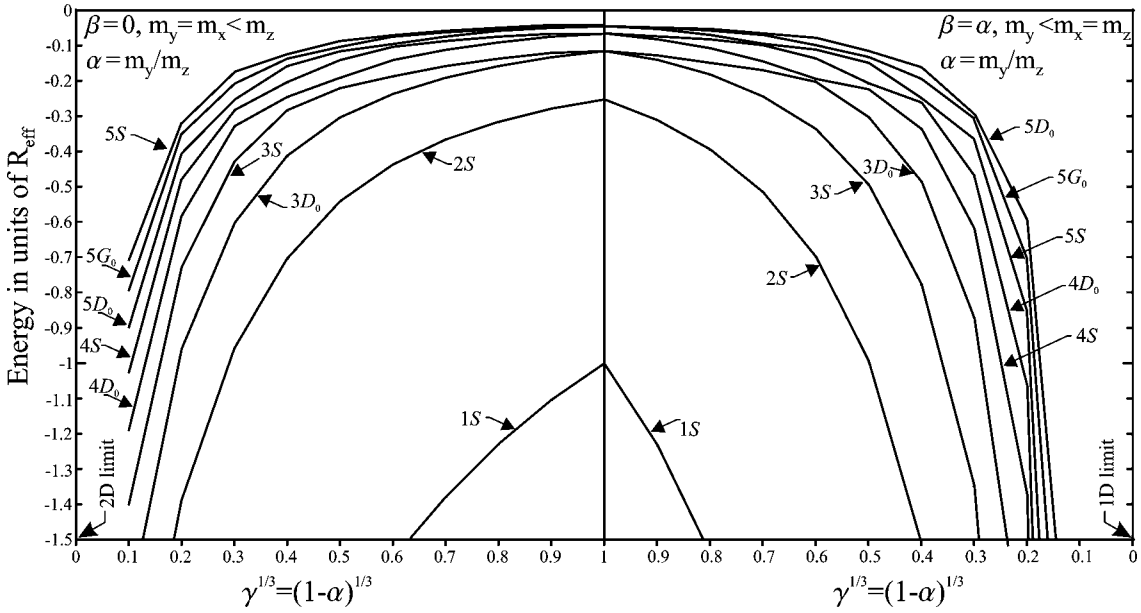

FIG. 2. Variation of the lowest-lying S-like states ($l=m=0$) with the parameter γ for the two cases of cylindrical symmetry, $\beta=0$ (to the left) and $\beta=\alpha$ (to the right). The energy scale is the same as in Ref. 2.

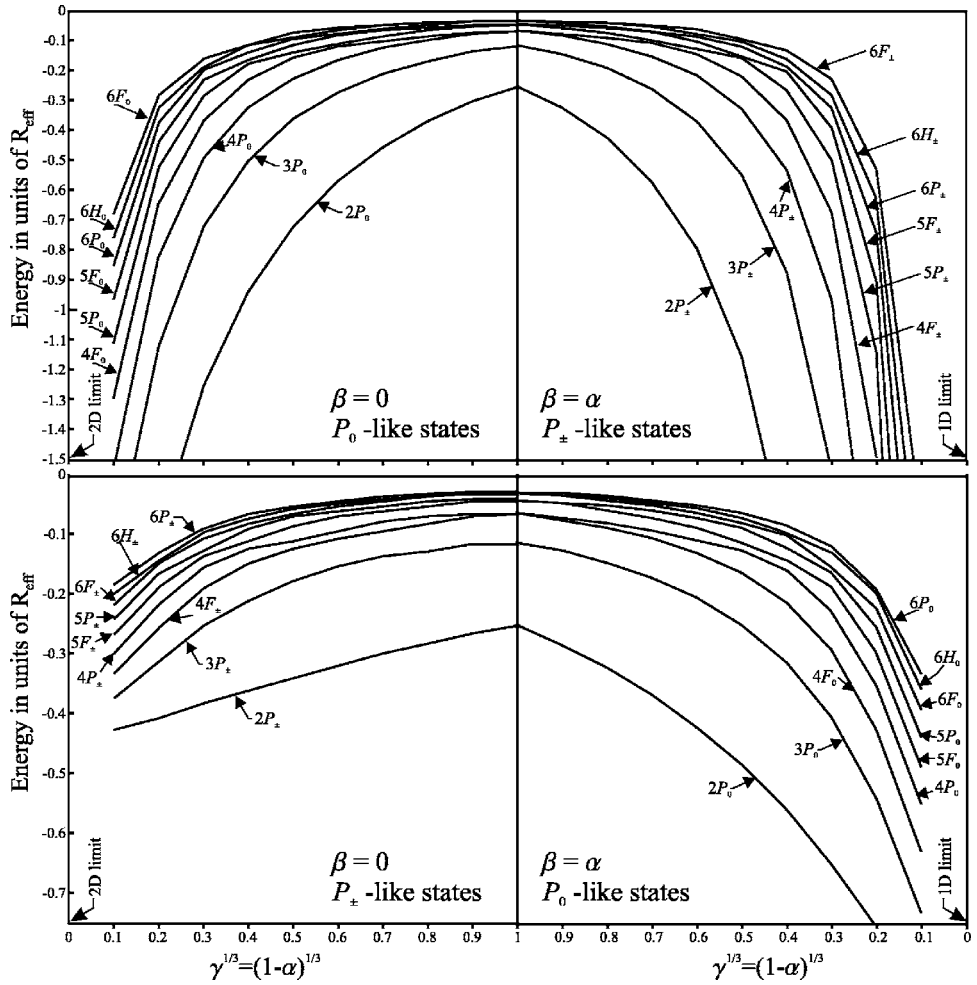

FIG. 3. Variation of the lowest-lying P-like states (as denoted in each part of the figure) with the parameter γ for the cylindrically symmetric cases. The energy scales are similar to those in Ref. 2.

spherical harmonic with maximum weight in the expansion of the corresponding wave function for values of γ close to 1 (the spherically symmetric case). Thus, in contrast to Ref. 2, the $3D_0$-like state has a larger binding energy than the $3S$-like state. However, the situation is reversed for $\beta=\alpha$. This discrepancy is, however, formal, and is a question of convention. Indeed, for smaller values of γ the weight of the spherical harmonic with $l=2$ (corresponding now to $4D_0$), in fact becomes larger also for the higher state. Thus, the notations should be comprehended as entirely formal.

Note that all binding energies vary linearly with α for small values of α ($\gamma\rightarrow 1$ from both sides of the graph), as predicted by the perturbation theory.[3] Thus, the "first derivative" appears disrupted at $\alpha=0$, which might look as a disagreement with the graphs in Ref. 3. Recall, however, that our definition of α (for $\beta=\alpha$) is different from the one in Ref. 3, which results in a different definition of R_{eff}. In our definition R_{eff} always involves the smaller mass, whereas in Ref. 3 it involves the duplicated mass, which is also the larger one when $\beta=\alpha$. Thus, as the larger masses increase and tend to infinity when the one-dimensional case is approached, their effective Rydberg also tends to infinity, whereas it is constant in our case. This explains the different appearance of our graphs from those in Ref. 3.

2. General case

The energies of the six lowest states calculated for a set of values of α and β are presented in the tables of Ref. 16. The calculation is performed for the fully-symmetric (S-like) states of even parity (Γ_1^+ symmetry), and for the odd parity P-like states (Γ_3^-, Γ_2^-, and Γ_4^- symmetries), to which optical transitions from the ground state are parity allowed. The values for $\gamma^{1/3}=0.1$, 0.2 are not included since their accuracy is insufficient with $L_{\max}=12(13)$. The common notations for the states (e.g., $1S$, $2P_0$, etc.) are not always applicable, that is why each state in these tables is labelled with a subscript, showing the values (l,m) of the radial function U_l^m with largest weight in the norm of the wave function.

Note that when the cylindrically symmetric cases $\beta=0$ and $\beta=\alpha$ are computed with the larger Hamiltonian matrix (involving all allowed values of m), apart from the slight discrepancy (mostly for $\gamma^{1/3}=0.3$) easily understood as due to the restricted value of $L_{\max}$, some new eigenvalues appear in-between [e.g., the value of 0.0691 between the values 0.0724 and 0.0492 in the P_0-like states for $\gamma^{1/3}=0.9$, $\beta=0$ (cf. Table II in Ref. 16 and Table II)]. A simple inspection of the wave functions shows that this is actually the $4F_{\pm 2}$ state ($l=3$, $m=2$), which is of course not calculated when only $m=0$ is used. However, it will be seen that these additional values are important in the following discussion.

It is interesting to trace the behavior of the P-like states when α is fixed and β increases from zero to α. This variation is illustrated in Fig. 4 for $\gamma^{1/3}=0.9$. The curves corresponding to a triplet of states (e.g., $2P_0$, $2P_+$, and $2P_-$) describe a zigzag as β varies from the one cylindrically symmetric case to the other. At $\beta=0$, the $2P_+$ and the $2P_-$ states merge into the $2P_\pm$ state, and the latter has lower binding energy than the corresponding $2P_0$state, because the lobes of the $2P_0$ wave function are extended along the spatial

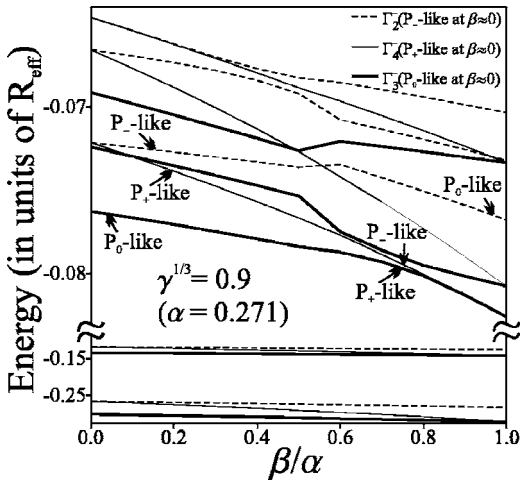

FIG. 4. Variation of the binding energies of the odd-parity P-like states with the ratio β/α for an arbitrarily chosen value of the parameter $\alpha=0.271$ ($\gamma^{1/3}=0.9$). Note the axis brake and the expanded scale in the upper part of the figure. A triplet of states is marked with notations which are only valid for $\beta\rightarrow 0$ or $\beta\rightarrow\alpha$, as discussed in text.

direction corresponding to the largest effective mass, i.e., Oz ($m_z>m_x=m_y$). The increase of β from zero to α can be viewed as increase of m_x from the value equal to m_y to the value equal to m_z. Therefore, the corresponding P_+ state (with lobes along the Ox axis) will increase its energy faster than the other two states in order to reach at $\beta=\alpha$ the state of largest energy, i.e., the "former" P_0. However, at $\beta=\alpha$ this latter state cannot be classified as P_0-like anymore, because it merges with the former P_+ to form the $P_\pm$-like state of the cylindrically symmetric case $\beta=\alpha$. The third state, which was the P_--like state for $\beta\rightarrow 0$, becomes the P_0-like state as $\beta\rightarrow\alpha$, and it now has lower energy than the other two because its lobes are extended along the Oy axis. This is clearly repeated throughout all the P-like states for any value of γ, although zigzags corresponding to higher states may intersect in quite a complicated pattern, as can be seen on the enlarged scale in the upper part of Fig. 4.

The above consideration also shows how formal are the notations used for the states. They are meaningful only for small deviations of β from zero or α. That is why subscript labels are used in the tables of Ref. 16. Note that the values of m in the subscripts of Table II in Ref. 16 change from even to odd in each column at some point, and similarly, from odd to even in Table III. This is a consequence of the alternative use of two coordinate systems ($Oxyz$ and $Ox'y'z'$ in Fig. 1), and will be explained in Sec. II D.

D. Accuracy of the model

In this section we consider the influence of the different approximations made in order to obtain a finite Hamiltonian matrix on the accuracy of the solutions. In the process of calculation we have found that the $1S$ ground state and, to a much smaller extent, the $2S$ state are slightly influenced by the step h used to calculate the derivatives. This is so because the 1S state is the one with most rapidly changing

amplitude within one unit cell and its derivative needs more accurate evaluation. Decreasing h by a factor of 5 (e.g., by choosing $\rho_{\max}=30$ instead of 150) results in a slight increase of the binding energy of the $1S$ state (however, well below 1% for all γ). The correction for $2S$ is much smaller, nevertheless, these more accurate values for $1S$ and $2S$ are given in all tables. The rest of the states are calculated with $\rho_{\max}=150$. If the step is decreased by a factor of 2 (by choosing $N_r=4096$ instead of 2048 and keeping $\rho_{\max}=150$), the most noticeable changes are in the fourth digit (i.e., below 0.1%) of the $1S$ states corresponding to $\gamma=0.1$ close to the one-dimensional case ($\beta\sim\alpha$). Thus, in all calculations, $N_r=2048$ was considered sufficient for the number of digits displayed in the tables.

We have noticed no significant impact of the choice of $\rho_{\max}>150$ on the eigenvalues, hence the value $\rho_{\max}=150$ can be considered as sufficiently large for the first 10 (or so) excited states. This is justified by the nature of the problem (all wave functions for bound states are finite) and our calculation. Indeed, each wave function decays from its maximum by several orders of magnitude towards $\rho=\rho_{\max}=150$.

The largest impact on the accuracy comes from the restriction of the series expansion of the wave function to values of $l\leqslant L_{\max}$. Smaller values of γ require larger $L_{\max}$, which is, however, limited by the size of the resulting Hamiltonian matrix. While the cylindrically symmetric cases can be computed with sufficient accuracy for all values of γ given in Table II, the accuracy in the general case is sometimes worse. We already noticed that as β increases from 0 to α (for any given α) we must switch from the spherical harmonics in the original Cartesian coordinate system (CCS) to the corresponding harmonics in the primed system (CCS′, cf. Fig. 1). We suggest that the switching occurs at the value of β_α, which satisfies the equation

$$\beta_\alpha=\frac{(\alpha-\beta_\alpha)}{(1-\beta_\alpha)}, \tag{14}$$

and which depends on alpha. In terms of the effective masses Eq. (14) is equivalent to $m_x=\sqrt{m_y m_z}$. This value is chosen because of the following reasoning. From the series expansions used for calculation of the matrix elements, Eqs. (A5) and (A7)), it is clear that the leading term in the series has a maximum value β if CCS is used, and $(\alpha-\beta)/(1-\beta)$ if CCS′ is used. It is desirable to use the smaller of these quantities in order to minimize the contribution of the series in the value of the outer integral and, consequently, the mixing of states with different values of m, hence the above equation. The worst accuracy is expected near β_α, however we have found that the disparity between the eigenvalues calculated in CCS and CCS′ near this point, being largest at $\gamma^{1/3}=0.3$ ($\sim$9%), rapidly decreases, as expected, with increasing γ (below 1% for $\alpha<0.7$).

We note that both approximations considered above lead to the fact that the obtained eigenvalues are upper bounds to the true ones. This is quite obvious for the truncation of the wave functions above $\rho_{\max}$, since not including the (infinite) region of space beyond $\rho_{\max}$ leads to not accounting for the integral of the wave function amplitudes in that region, which is involved in the calculation of the energy, i.e., the calculated energies are upper bounds to the true ones. On the other hand, decreasing $L_{\max}$ leads to smaller Hamiltonian matrices, which can be viewed as obtained from the larger one by subsequently removing the last row and the last column. According to a well-known theorem,[17] the eigenvalues of the smaller matrices are always upper bounds to the eigenvalues of the large one and, hence, in the limit $N\to\infty$, to the true ones.

III. COMPARISON WITH OTHER CALCULATIONS AND EXPERIMENT

A. Comparison with other models

To the best of our knowledge, other models presented so far in the literature are all concerned with the cylindrically symmetric cases. The calculation performed by Faulkner covers only the case (in our notations) $\beta=0$ and needs revision due to the restricted set of basis functions used. For germanium ($\gamma^{1/3}\approx 0.39$), where the errors in Faulkner's calculation are much more significant than for silicon, the calculation has been repeated by Beinikhes *et al.*[18] The nonvariational method used by them is equivalent to ours, but the method of obtaining the eigenvalues and the eigenvectors of the large Hamiltonian matrix is different.[19] They have used $L_{\max}=10(11)$, which seems to be enough for Ge, since their results[18] coincide almost exactly with our calculation for Ge (not shown) with $L_{\max}=28(29)$. However, we note that if we use the high-resolution data in Refs. 20 and 21 and apply the least square fit as explained in the next section in order to obtain the donor ground-state energy and the value of the dielectric constant, we get $\varepsilon=15.0$ instead of $\varepsilon=15.4$, which was used in Ref. 18. If older data (containing, however, less observed transitions) is used,[22] then the least square fit indeed yields $\varepsilon=15.4$, as obtained by Faulkner.[2]

It is interesting to look to the approximate analytical formula proposed by Gerlach and Pollmann[3] from the point of view of our model. If all terms with $(l',m')\neq(l,m)$ in the system of differential equations (11) is neglected, the equations decouple and the equation for $U_l^m(\rho)$ can be easily brought to the following form:

$$\frac{d^2U_l^m}{dz^2}+\left(-1+\frac{2\eta}{z}-\frac{l(l+1)}{z^2}\right)U_l^m=0, \tag{15}$$

where $z=\sqrt{|\epsilon|}\rho$, and $\eta=Z_{ll}^{mm}/\sqrt{|\epsilon|}$. This is the differential equation for Coulomb functions. The solutions describing bound states (called also negative energy solutions) are given by the Whittaker function $W_{\eta,l+1/2}(2z)$,[23] and using arguments similar to those in Ref. 10 it is possible to show that the parameter η must be a positive integer for the solution to be acceptable as a wave function (i.e., to have a finite derivative at the origin). Denoting this integer by n, we obtain exactly the approximate formula of Gerlach and Pollmann,[3]

$$|E|=|\epsilon|R_{\text{eff}}=R_{\text{eff}}\frac{(Z_{ll}^{mm})^2}{n^2} \tag{16}$$

(of course, $E=-|E|=E_{(nl)m}$, the latter being the original notation).[3] Thus, the above formula, obtained in Ref. 3 using

the first nonvanishing correction from the perturbation theory, is equivalent to the assumption that there is no mixing of the states. It is, therefore, expected to give a good estimation of the binding energies only in the case of small anisotropy, and only for some low-lying states, for which the mixing indeed can be neglected. In any case, the absolute value of the energy will be underestimated. Thus, for example, for InSe the following transition energies from the $1S$ state have been calculated using Eq. (16):[24] 102 cm^{-1} ($1S-2P_{\pm}$), 114 cm^{-1} ($1S-2P_0$), and 124 cm^{-1} ($1S-3P_{\pm}$). The correct values are 104, 115.4, and 126 cm^{-1}, respectively. Note, that InSe corresponds to the cylindrically symmetric case with $\beta=\alpha\approx 0.56$ in our notations ($\alpha' \approx -1.3<0$), so that Faulkner's tables are not applicable.

Finally, formula (16) can obviously be applied also to the general case (general $\beta\neq\alpha$ and $\beta\neq 0$), but *only* for states which are almost "pure" (i.e., almost the whole contribution to the norm of the wave function is due to a single U_l^m). However, in this case the matrix elements must be calculated numerically, and, in addition, there is no prescription to find out *a priori* which states are pure and which do exhibit significant mixing.

B. Comparison with absorption data for 4*H*-SiC

Absorption data on the nitrogen-donor excited states is available for 3*C*-,[25] 4*H*-,[26,27] and 6*H*-SiC.[28] The data for 3*C*-SiC (a cubic crystal) is treated in the frame of Faulkner's theory and is in excellent agreement with it. To the best of our knowledge, so far 4*H*-SiC is the only uniaxial crystal with parabolic conduction band, for which the general theory is applicable, and a preliminary account on this application was presented recently,[5] illustrating a very good agreement with the available experimental data (cf. Fig.1 in this reference). Since only few excited states were computed at that time (assuming the value $\varepsilon=\sqrt{\varepsilon_{\perp}\varepsilon_{\parallel}}=9.95$), and fitting (see below) was not used, we justify and provide a more complete set of binding energies here.

When fitting the theoretical data to the data from Ref. 26 (showing the sharpest transitions), we did not assume any value for ε but, instead, used the least-square method to obtain its value and the binding energies of the ground state $1S(\Gamma_2)$ and its counterpart $1S(\Gamma_3)$, which provide the least sum of the squares of the deviations between the experimental and theoretical binding energies. (Note that the energy unit, R_{eff}, also needs evaluation since it depends on ε.) This results in the following formulas:[29]

$$R_{\mathrm{eff}} = -\frac{\sum_{i=1}^{K} \triangle\epsilon_i(\bar{E}_1 - E_{1i} + \bar{E}_2 - E_{2i})}{2\sum_{i=1}^{K} \triangle\epsilon_i^2},$$

$$E_J = R_{\mathrm{eff}}\bar{\epsilon} + \bar{E}_J, \quad J=1,2,$$

$$\varepsilon = \sqrt{\varepsilon_{\perp}\varepsilon_{\parallel}} = \sqrt{m_y/R_{\mathrm{eff}}}, \tag{17}$$

where we use the notations

$$\triangle\epsilon_i \equiv \bar{\epsilon} - \epsilon_i,$$

$$\bar{\epsilon} = \frac{1}{K}\sum_{i=1}^{K}\epsilon_i,$$

$$\bar{E}_J = \frac{1}{K}\sum_{i=1}^{K} E_{Ji}, \quad J=1,2.$$

Here $E_1 \equiv E_{1S(\Gamma_2)}$ and $E_2 \equiv E_{1S(\Gamma_3)}$ denote the binding energies of $1S(\Gamma_2)$ and $1S(\Gamma_3)$, respectively, ϵ_i is the calculated eigenvalue corresponding to the *binding* energy of the final state involved in the ith experimentally observed transition, E_{1i} and E_{2i} are the experimental *transition* energies from $1S(\Gamma_2)$ and $1S(\Gamma_3)$, respectively, to the ith final state, and K is the number of the observed transitions, which happens to be the same, $K=4$, for transitions starting from $1S(\Gamma_2)$ and from $1S(\Gamma_3)$ (transitions to $2P_0$, $2P_-$,$3P_0$, and $3P_-$ from both initial states are observed).[5] It is important to note that the identification of the final states in the experimentally observed transitions must be known before applying the fit. The values $\varepsilon=9.93\pm0.01$, $E_{1S(\Gamma_2)}=61.37\pm0.1$ meV, and $E_{1S(\Gamma_3)}=53.9\pm0.1$ meV are obtained from the fit.

The calculated binding energies for the 10 lowest states of each symmetry using the value of $\varepsilon=9.93$ from the fit are presented in Table III. The notations used in Table III are similar to those used by Faulkner,[2] however, some clarification is needed. Since the values $+m$ and $-m$ always enter the wave function on equal footing, we omit the sign ± in front of the subscript denoting the value of m. Thus, for example, $D_{\pm 2}$ becomes simply D_2. However, since the $P_{\pm}$-like states are split for $\beta\neq 0$, we retain a "+" (or "–") sign *after* the subscript m, which simply denotes the split-off state with larger (smaller) energy, respectively. As usual, the value of $m=1$ is not written, so, for instance, $P_{\pm}$ splits into P_+ and P_-, etc. The identification of the experimentally observed transitions has been carried out in Fig. 1 and Table 2 of Ref. 5 and will not be repeated here.

Since the envelope functions are known from the calculation, it is interesting to inspect the transition probabilities, which within the EMT are proportional to the integrals[30]

$$I_{if} = (E_i - E_f)\int \phi_i x_{\alpha}\phi_f dV, \tag{18}$$

where ϕ_i and ϕ_f are the envelope wave functions of the initial and final states, respectively, x_{α} is the coordinate in the direction of the polarization of the photon causing the transition. The integration is over the whole space. The presence of three equivalent conduction band minima is taken into account and the multivalley envelope functions needed in the calculation are constructed as linear combinations (in accord with Ref. 4) of the one-valley functions calculated here.[30] The initial state is always $1S$, and since the contribution of U_0^0 in this state is almost 100% (99.85%), without significant loss of precision ϕ_i can be approximated with $[U_0^0(\rho)/\rho]Y_0^0(\theta,\varphi)=(2\sqrt{\pi})^{-1}U_0^0(\rho)/\rho$. The final state is one of the P-like states, P_0 or P_- for photon polarization $\mathbf{E}\perp\mathbf{c}$ and P_+ for $\mathbf{E}\parallel\mathbf{c}$.[4] Although the ground-state envelope function is

TABLE III. Calculated binding energies (in meV) of the lowest excited states of each symmetry for 4*H*-SiC using $\varepsilon=9.93$ and $m_y=0.31$ (in units of the electron rest mass). The notations of the states reflect the values l, m of the function U_l^m with maximum weight in the norm.

Γ_1^+ (S-like)		Γ_3^- (P_0-like)		Γ_2^- (P_--like)		Γ_4^- (P_+-like)		Γ_3^+		Γ_2^+		Γ_4^+		Γ_1^-	
$1S$	53.99	$2P_0$	15.67	$2P_-$	12.25	$2P_+$	12.79	$3D_2$	5.389	$3D_+$	6.404	$3D_-$	6.200	$4F_2$	3.358
$2S$	13.72	$3P_0$	7.046	$3P_-$	5.504	$3P_+$	5.735	$4D_2$	3.051	$4D_+$	3.636	$4D_-$	3.527	$5F_2$	2.167
$3D_0$	6.781	$4P_0$	4.044	$4F_-$	3.559	$4F_+$	3.672	$5G_2$	2.227	$5G_+$	2.400	$5G_-$	2.334	$6H_2$	1.580
$3S$	5.998	$4F_0$	3.649	$4P_-$	3.114	$4P_+$	3.238	$5D_2$	1.963	$5D_+$	2.304	$5D_-$	2.232	$6F_2$	1.509
$3D_2$	5.386	$4F_2$	3.358	$4F_{3-}$	2.978	$4F_{3+}$	2.979	$5G_4$	1.886	$5G_{3+}$	2.078	$5G_{4-}$	2.078	$6H_4$	1.410
$4D_0$	3.901	$5P_0$	2.643	$4F_-$	2.297	$4F_+$	2.369	$6G_2$	1.555	$6G_+$	1.693	$6G_-$	1.649	$7H_2$	1.172
$4S$	3.335	$5F_0$	2.319	$5P_-$	2.001	$5P_+$	2.077	$6D_2$	1.370	$6D_+$	1.590	$6D_-$	1.540	$7F_2$	1.109
$4D_2$	3.046	$5F_2$	2.166	$5F_{3-}$	1.913	$5F_{3+}$	1.914	$6G_4$	1.313	$6G_{3+}$	1.452	$6G_{3-}$	1.452	$7H_4$	1.041
$5D_0$	2.552	$6P_0$	1.856	$5F_-$	1.630	$5F_+$	1.678	$7I_2$	1.175	$7G_+$	1.264	$7G_-$	1.233	$8H_2$	0.913
$5G_0$	2.347	$6H_0$	1.649	$6H_-$	1.571	$6H_+$	1.622	$7G_2$	1.140	$7I_+$	1.209	$7I_-$	1.173	$8J_2$	0.893

quite inaccurate within the EMT, we anticipate that the deviation from the real one is more important mainly in the vicinity the donor core. Since the contribution from that region in the integrals of Eq. (18) is minor (all P-like states have vanishing amplitudes at the origin), we may expect that the calculated values will be accurate enough for comparison to experimental data.

The calculated transition probabilities are given in Table IV. They should be compared to the intensities of the absorption lines.[27] Unfortunately, the quality of these absorption spectra does not allow precise determination of the intensities (the samples are different from those used in Ref. 26), but a qualitative comparison with the theory is still possible. Thus, it is quite obvious that the transitions to $2P_0$ and $2P_-$ from both $1S(\Gamma_2)$ (the lines at 367 and 397 cm^{-1} in this reference) and $1S(\Gamma_3)$ (the lines at 307 and 337 cm^{-1}) have almost equal intensities, in agreement with theory (cf. Fig. 2, $\mathbf{E}\perp\mathbf{c}$, in Ref. 27). Also the line at 450 cm^{-1}, identified as $1S(\Gamma_2)$-$3P_-$ is likely to have the intensity predicted by the theory, about 21% of the stronger lines. The corresponding transition $1S(\Gamma_3)$-$3P_-$ is not resolved, probably due to overlapping with the strong $1S(\Gamma_2)$-$2P_-$ line. Furthermore, the transitions at 388 and 455 cm^{-1} with $\mathbf{E}\|\mathbf{c}$ are most probably dominated by $1S(\Gamma_2)$ – $2P_+$ and $1S(\Gamma_2)$-$3P_+$, respectively, and their intensity ratio is also in qualitative agreement with the theory. The anticipated $1S(\Gamma_3)$-$2P_+$ transition, which should be observed at higher temperatures, is probably appearing just as a shoulder on the high-energy side of the strong 388 cm^{-1} peak. Finally, the comparison of the absorption intensities with $\mathbf{E}\|\mathbf{c}$ and $\mathbf{E}\perp\mathbf{c}$ carried out in Fig. 4 of Ref. 27 shows that the intensity of the absorption with $\mathbf{E}\|\mathbf{c}$ in the transitions to the $2P_+$ state from both $1S(\Gamma_2)$ (388 cm^{-1})and $1S(\Gamma_3)$ (328 cm^{-1}) is indeed about 2 times stronger than the corresponding lines with $\mathbf{E}\perp\mathbf{c}$ (the transitions to either $2P_0$, or to $2P_-$), in agreement with Table IV.

TABLE IV. Theoretical probabilities for transitions from the ground $1S$ state to the excited states listed. All values are normalized to the probability of the $1S$-$2P_0$ transition.

$2P_0$	$3P_0$	$2P_-$	$3P_-$	$2P_+$	$3P_+$
1.0	0.20	0.98	0.21	2.18	0.50

A special remark is necessary for the absorption spectrum with $\mathbf{E}\|\mathbf{c}$ (Fig. 2 of Ref. 27). It was already shown[4] that transitions between the S-like states with the same symmetry (Γ_2 or Γ_3) are symmetry allowed, although they are parity forbidden. Calculation of their intensities cannot be attempted without knowledge of the exact Bloch function at the conduction band minimum, but theoretically they lie very close in energy to the P_+-like states (cf. Table III) and might be responsible for the large linewidths observed with $\mathbf{E}\|\mathbf{c}$.

IV. CONCLUSIONS

The investigated nonvariational method for numerical solution of the effective-mass Schrödinger equation has the obvious advantage before the variational method that no trial functions are needed; in fact, the iterations for finding the eigenvalues and the eigenvectors of the Hamiltonian matrix are started with a randomly generated vector. The calculated eigenvalues have a good enough precision in a broad region of variation of the anisotropy parameters α and β. We have shown, however, that the results have to be treated with caution in some cases ($\alpha\to 1$ and $\beta\approx\beta_\alpha$), when strong mixing of states of different m occurs. This is always the case for values of α very close to one, but even in this case a reasonable accuracy for the lowest excited states can be achieved using large enough values of $L_{\max}$. We believe that most practical cases can be handled with values of α well below one, as is the considered case of 4*H*-SiC. The theory seems to be in a very good agreement with the experiment in this case. However, a much more detailed comparison will be possible when spectra measured in the future on samples of better quality and/or other anisotropic materials will show sharper lines and more excited states. The experimental accuracy of the values of the effective masses in 4*H*-SiC (about ±2% at present) also needs improvement. So far, the accuracy of the theory is superior to that of the experiment.

ACKNOWLEDGMENT

Support from the Swedish Research Council is gratefully acknowledged.

APPENDIX: CALCULATION OF THE MATRIX ELEMENTS

The matrix elements are defined by Eq. (12), in which the anisotropy function f is given by Eq. (8a) if the calculation is to be performed in CCS, and by Eq. (8b) if CCS′ is to be used. In any case, f can be expanded in Taylor series:

$$f(\theta,\varphi)=\frac{1}{\sqrt{1-\alpha\cos^2\theta}}\sum_{n=0}^{\infty}a_n\left(\frac{\beta\sin^2\theta\cos^2\varphi}{1-\alpha\cos^2\theta}\right)^n, \quad \text{(A1)}$$

$$f(\theta',\varphi')=\frac{1}{\sqrt{1-\beta\sin^2\theta'}}\sum_{n=0}^{\infty}a_n\left(\frac{(\alpha-\beta)\sin^2\theta'\sin^2\varphi'}{1-\beta\sin^2\theta'}\right)^n, \quad \text{(A2)}$$

obtained directly from the expressions (8a) and (8b), respectively. Here $a_0=1$, $a_n=(2n-1)!!/2^n n!$, and it is easily verified that for $\beta<\alpha$ in (A1) and $\beta>1-\sqrt{1-\alpha}$ in (A2), which are the bounds for using CCS or CCS′, respectively, the corresponding series are converging by absolute values, since their terms are dominated by the terms of a geometrical progression. Feeding back the expansion in Eq. (12) and using the definition of the spherical harmonics, it can be noticed that the integration over φ can be performed analytically in order to obtain the subintegral function $F(\theta)$ [or $F(\theta')$] for the remaining integration over θ [or θ'] as a sum of rapidly converging series. Considering first the calculation within CCS, $F(\theta)$ has the following appearance:

$$F(\theta)=\frac{G_{ll'}^{mm'}(\theta)}{\sqrt{1-\alpha\cos^2\theta}}[\pm S_+(\theta)+S_-(\theta)]. \quad \text{(A3)}$$

The following notations are used:

$$G_{ll'}^{mm'}(\theta)=\sqrt{\frac{(2l+1)(l-m)!\,(2l'+1)(l'-m')!}{(l+m)!\,(l'+m')!}}\times P_l^m(\cos\theta)P_{l'}^{m'}(\cos\theta), \quad \text{(A4)}$$

where P_l^m, $P_{l'}^{m'}$ are the associated Legandre polynomials in a standard notation.

$$S_\pm(\theta)=\delta_{0,m\pm m'}+\sum_{n=1}^{\infty}a_n\left(\frac{\beta\sin^2\theta}{1-\alpha\cos^2\theta}\right)^n\times\frac{(2n)!}{2^{2n}\left(n+\frac{m\pm m'}{2}\right)!\left(n-\frac{m\pm m'}{2}\right)!}, \quad \text{(A5)}$$

where δ_{ij} is the usual Kronecker symbol. The sign ambiguities are resolved, as follows. In Eq. (A5) the sign is "+" for S_+ and "−" for S_-. In Eq. (A3), the sign in front of S_+ is "+", if m and m' are even and the expansion of the wave function involves $(Y_l^m+Y_l^{-m})$. It is also "+", if m and m' are odd, but the expansion of the wave function involves $(Y_l^m-Y_l^{-m})$, and the sign is "−" in the remaining cases. In other words, the sign in Eq. (A3) is "+" for wave functions transforming as Γ_1^+, Γ_2^+, Γ_3^-, and Γ_4^-, and "−" for the rest of the representations.

The series appearing in Eq. (A5) and, therefore, $F(\theta)$ can be evaluated easily with any desired precision (double precision was used), which ensures about 10 significant digits after the numerical integration over θ. The latter is done using the standard procedure DQDAWO from the IMSL Fortran 90 MP Library.

Finally, we list the corresponding formulas in CCS′.

$$F(\theta')=\frac{G_{ll'}^{mm'}(\theta')}{\sqrt{1-\beta\sin^2\theta'}}[\pm S_+(\theta')+S_-(\theta')], \quad \text{(A6)}$$

$$S_\pm(\theta')=\delta_{0,m\pm m'}+\sum_{n=1}^{\infty}(-1)^n a_n\left(\frac{(\alpha-\beta)\sin^2\theta'}{1-\beta\sin^2\theta'}\right)^n\times\frac{(2n)!}{2^{2n}\left(n+\frac{m\pm m'}{2}\right)!\left(n-\frac{m\pm m'}{2}\right)!}. \quad \text{(A7)}$$

[1] W. Kohn and J. M. Luttinger, Phys. Rev. **98**, 915 (1955).
[2] R. A. Faulkner, Phys. Rev. **184**, 713 (1969).
[3] B. Gerlach and J. Pollmann, Phys. Status Solidi B **67**, 93 (1975).
[4] I. G. Ivanov, B. Magnusson, and E. Janzén, Phys. Rev. B **67**, 165212 (2003).
[5] I. G. Ivanov, A. Stelmach, M. Kleverman, and E. Janzén, *Proceedings of 5th European Conference on Silicon Carbide and Related Materials* (August 31–September 4, 2004) [Mater. Sci. Forum **483-485**, 511 (2005)].
[6] C. Persson and U. Lindefelt, J. Appl. Phys. **82**, 5496 (1997).
[7] H. J. Mattausch and C. Uihlein, Phys. Status Solidi B **96**, 189 (1979).
[8] M. Said, M. A. Kanehisa, M. Balkanski, and Y. Saad, Phys. Rev. B **35**, 687 (1987).
[9] A. L. Thilderkvist, M. Kleverman, G. Grossmann, and H. G. Grimmeiss, Phys. Rev. B **49**, 14270 (1994).
[10] R. Loudon, Am. J. Phys. **27**, 649 (1959).
[11] See, e.g., J. F. Cornwell, in *Group Theory and Electronic Energy Bands in Solids*, edited by E. P. Wohlfarth (North-Holland, Amsterdam, London, 1969).
[12] G. F. Koster, J. O. Dimmock, R. G. Wheeler, and H. Statz, *Properties of the Thirty-Two Point Groups* (MIT Press, Cambridge, MA, 1963).
[13] For a discussion on the Lánczos method for solving large eigenvalue problems, see, e.g., J. K. Cullum and R. A. Willoughby, *Lánczos Algorithms for Large Symmetric Eigenvalue Computa-*

tions (Birkhäuser, Boston, Basel, 1985), Vol. 1.
[14] H. N. Spector and J. Lee, Am. J. Phys. **53**, 248 (1985).
[15] E. Janzén, R. Stedman, G. Grossmann, and H. G. Grimmeiss, Phys. Rev. B **29**, 1907 (1984).
[16] See EPAPS Document No. E-PRBMDO-73-078604 for the tables containing the calculation results in the general case. This document can be reached via a direct link in the online article's HTML reference section or via the EPAPS homepage (http://www.aip.org/pubservs/epaps.html).
[17] A. Jennings, *Matrix Computations for Engineers and Scientists* (Wiley, New York, 1977).
[18] I. L. Beinikhes and Sh. M. Kogan, in *Proceedings of the Third International Conference on Shallow Impurities in Semiconductors* (August 10–12, 1988, Linköping, Sweden), Inst. Phys. Conf. Ser. No. 95, edited by B. Monemar (IOP, Bristol, Philadelphia, 1989), p. 161.
[19] I. L. Beinikhes, Sh. M. Kogan, A. F. Polupanov, and R. Taskinboev, Solid State Commun. **53**, 1083 (1985).
[20] M. S. Skolnick, L. Eaves, R. A. Stradling, J. C. Portal, and S. Askenazy, Solid State Commun. **15**, 1403 (1974).
[21] S. D. Seccombe and D. M. Korn, Solid State Commun. **11**, 1539 (1972).
[22] R. L. Aggarwal, P. Fisher, V. Mourzine, and A. K. Ramdas, Phys. Rev. **138**, A882 (1965).
[23] M. Abramowitz and I. A. Segun, *Handbook of Mathematical Functions* (Dover, New York, 1965).
[24] J. Martinez-Pastor, A. Segura, C. Julien, and A. Chevy, Phys. Rev. B **46**, 4607 (1992).
[25] W. J. Moore, P. J. Lin-Chung, J. A. Freitas, Jr., Y. M. Altaiskii, V. L. Zuev, and L. M. Ivanova, Phys. Rev. B **48**, 12289 (1993).
[26] C. Q. Chen, J. Zeman, F. Engelbrecht, C. Peppermüller, R. Helbig, Z. H. Chen, and G. Martinez, J. Appl. Phys. **87**, 3800 (2000).
[27] C. Q. Chen, R. Helbig, F. Engelbrecht, and J. Zeman, Appl. Phys. A: Mater. Sci. Process. **A72**, 717 (2001).
[28] See F. Engelbrecht, S. Huant, and R. Helbig, Phys. Rev. B **52**, 11008 (1995), and the references therein.
[29] The first equation in Eqs. (17) is written for the case when transitions starting from two energy levels E_1 and E_2 are considered. If more starting levels (say, I) are included, its generalization is quite obvious for the sum in the numerator but the factor of 2 in the denominator has to be replaced by I.
[30] W. Kohn, Solid State Phys. **5**, 257 (1957). We use Eq. (5.56) of this reference.